SARCOIDOSIS VASCULITIS AND DIFFUSE LUNG DISEASES 2025; 42 (2): 16539 DOI: 10.36141/svdld.v42i2.16539

EBUS/EUS-guided lymph nodal gadolinium injection and MRI of the chest in diagnosis of abnormal lymphatic drainage. A case series

Venerino Poletti [1,2,3], *Simone Petrarulo*[2], *Emanuela Giampalma*[1,4], *Claudia Ravaglia*[1,2], *Sara Piciucchi*[1,4]

[1]Department of Medical and Surgical Sciences (DIMEC), Bologna University; [2]Pulmonology Unit, G.B. Morgagni Hospital, Forlì, Italy; [3]Department of Respiratory Diseases and Allergy, Aarhus University Hospital, Aarhus, Denmark; [4]Department of Radiology, GB Morgagni-Pierantoni Hospital, Italy

Abstract. Mediastinal lymphatic circulation may be disrupted as a consequence of congenital malformations, traumatic injury, or neoplastic infiltration. Such dysfunction can lead to a spectrum of clinical manifestations, most notably chylothorax, plastic bronchitis, and/or alveolar fatty pneumonitis. Although lymphography—traditionally involving the injection of contrast agents into peripheral lymph nodes—was historically utilised for diagnostic purposes, its application has been limited by considerable technical demands and challenges in image interpretation. Herein, we describe three cases of patients admitted to our institution with heterogeneous clinical presentations, including recurrent chylothorax, alveolar fatty pneumonitis, plastic bronchitis, and/or respiratory failure. A definitive diagnosis was established through the administration of 2 mL of gadolinium-based contrast medium into mediastinal lymph nodes under either endobronchial ultrasound (EBUS) or endoscopic ultrasound (EUS) guidance, with magnetic resonance imaging (MRI) performed both prior to and following the injection to evaluate contrast distribution.

The lymphatic system constitutes an integral component of the circulatory system, fulfilling essential physiological roles including nutrient transport, maintenance of fluid homeostasis, waste clearance, and immune surveillance and response (1–3).

Impairment of lymphatic circulation may arise from congenital anomalies, conduction defects secondary to infiltrative or traumatic injury, or a combination of these etiologies. Such dysfunction is associated with a range of clinical manifestations, including chylothorax, plastic bronchitis, alveolar fatty pneumonitis, protein-losing enteropathy, and chylous ascites (4–6).

A variety of imaging modalities have been employed to visualise lymphatic anatomy and flow dynamics; however, these techniques have historically been limited by poor spatial resolution, suboptimal opacification of lymphatic structures, and challenges in accurately delineating lymph flow. Recent advancements in imaging have been made possible through the synergistic use of high-resolution magnetic resonance imaging (MRI) and soft tissue contrast enhancement, enabled by the administration of contrast agents via peripheral lymphatic routes—most commonly through the inguinal lymph nodes or hepatic lymphatic vessels. Among these, dynamic contrast-enhanced magnetic resonance lymphangiography (DCMRL) has emerged as a promising technique, allowing for detailed assessment of central lymphatic pathways following contrast injection into inguinal lymph nodes (7–10).

Received: 1 November 2024
Accepted: 19 January 2025
Correspondence: Dr. Sara Piciucchi
Department of Medical and Surgical Sciences (DIMEC), Bologna University/Department of Radiology, GB Morgagni-Pierantoni Hospital, Italy
Phone: +39 0543 735863
E-mail: piciucchi.sara@gmail.com

Irrespective of the underlying pathology, the most frequently observed imaging findings include delayed or absent contrast transit from peripheral to central lymphatics, extravasation into retroperitoneal, peritoneal, pleural, or pericardial compartments, and dilated or abnormally filled lymphatic channels due to malformations (6–12).

In this context, we propose a novel imaging approach involving direct gadolinium-based contrast injection into mediastinal lymphatic pathways under endobronchial or endoscopic ultrasound (EBUS/EUS) guidance, combined with pre- and post-contrast MRI (Siemens Aera, Erlangen, Germany). In cases where thoracic lymphatic drainage abnormalities were suspected, 2 mL of undiluted gadoteric acid (Dotarem; Guerbet, France) were slowly administered into the most caudally visualised mediastinal lymph nodes (level 8, or alternatively level 7) under EBUS or EUS guidance, with careful attention to avoid inadvertent contrast medium leakage into the esophageal or tracheobronchial lumen.

Pre-procedural MRI of the chest was performed to obtain baseline imaging, followed by post-procedural MRI using T1-weighted, breath-hold spoiled gradient echo sequences (DIXON technique) in both phases.

Case 1

A 54-year-old woman under follow-up for both squamous cell carcinoma and melanoma was referred to our clinic following a chest computed tomography (CT) scan that revealed mediastinal lymphadenopathy, pericardial effusion, and left-sided pleural effusion. Over recent months, she had reported progressive exertional dyspnoea. Ultrasonography confirmed the presence of left pleural effusion, and diagnostic thoracentesis yielded pink, turbid fluid. Biochemical analysis was consistent with chylothorax, showing a triglyceride concentration of 14.62 mmol/L. Cytological examination of the pleural fluid, as well as findings from fluorodeoxyglucose positron emission tomography (FDG-PET), were non-contributory.

After six months, due to worsening symptoms, the patient underwent medical thoracoscopy, which revealed a whitish thickening of the left parietal pleura. Histological analysis of pleural biopsies demonstrated nonspecific chronic inflammation. Given the persistence of chylothorax, an attempt was made to perform dynamic contrast-enhanced magnetic resonance lymphangiography (DCMRL) via inguinal intranodal gadolinium injection; however, the procedure was unsuccessful due to the small calibre of the lymph nodes.

Subsequently, we proceeded with endoscopic ultrasound (EUS)-guided administration of 2 mL of gadolinium into level 8, followed by magnetic resonance (MR) imaging. Pre-contrast T1- and T2-weighted sequences (Siemens AERA, Erlangen, Germany) were acquired, with post-contrast T1-weighted images obtained at 30 minutes and 1 hour after administration. The post-contrast MRI revealed a diffuse hyperintense signal within the entire left pleural effusion and a minimal right-sided effusion (Figure 1), suggestive of thoracic lymphatic leakage at a level just above T5—corresponding to the anatomical region where the thoracic duct typically crosses from right to left.

No definitive aetiology was identified; however, the patient was managed conservatively with a low-fat diet and monitored closely. At two-year follow-up, she remained in good clinical condition, with no recurrence of pleural effusion.

Case 2

A 63-year-old male with a history of occupational exposure to industrial powders presented with recurrent episodes of respiratory failure secondary to interstitial pneumonia of unclear aetiology over a 15-year period. Laboratory investigations consistently yielded negative results for autoimmune diseases, and microbiological analyses were non-contributory. High-resolution computed tomography (CT) of the chest demonstrated bilateral, extensive alveolar ground-glass opacities with a "crazy-paving" pattern, diffuse bronchial wall thickening, and mucus plugging (Figure 2). Additionally, the mediastinum and hila revealed hypodense, multiloculated fluid-density nodules.

As both dyspnoea and radiological findings progressively worsened, the patient underwent video-assisted thoracoscopic surgery (VATS) with lung biopsy. Histopathological analysis revealed intra-alveolar accumulation of faint periodic acid–Schiff (PAS)-positive material and the presence of foamy macrophages—features not typical of pulmonary alveolar proteinosis. Postoperatively, the patient developed a chylothorax, which was managed conservatively with chest tube drainage.

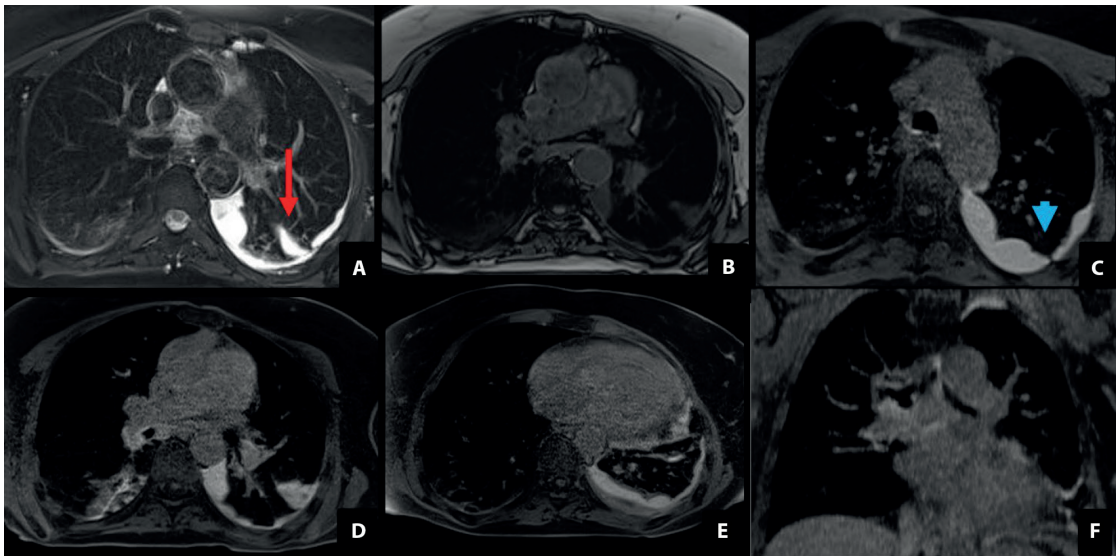

Figure 1. T2 weighted TSE with motion correction- BLADE (a) shows loculated effusion in the left pleural space and in the fissure (red arrow). Minimal fluid is present also in the right side. T1-w GRE-VIBE (b) sequence shows low signal of the pleural effusion. T1-w with fat saturation (c-f) after endoscopic contrast medium injection shows high signal of the pleural effusion (c, blue arrow-head).

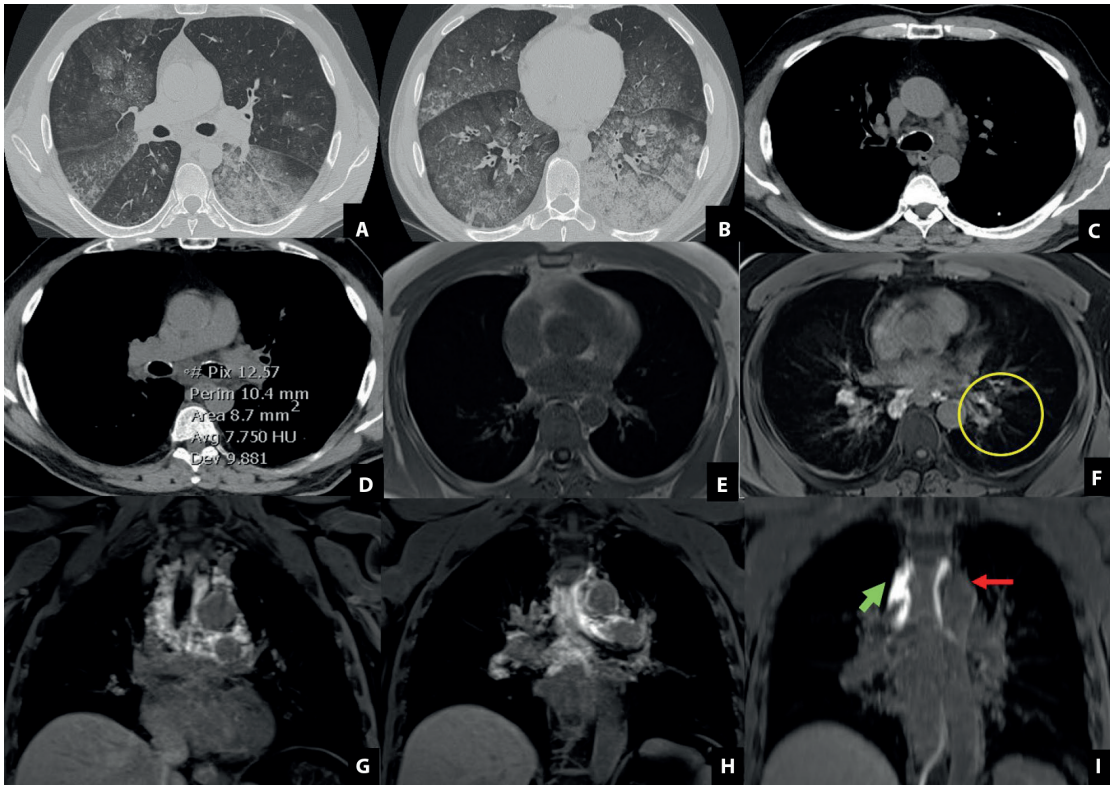

Figure 2. CT scan (a-d) shows extensive bilateral ground glass attenuation and crazy paving pattern, associated with consolidation in the left lower lobe. Diffuse thickening of the bronchial wall is also present (a-b). In the mediastinal window (c,d) multiple nodular structures with fluid density (d) are present in all the mediastinal and hilar stations. MRI T1-weighted sequence before contrast (e). T1-w after injection of contrast medium (f-i) shows high signal in all the mediastinal structures. The peribronchovascuar interstitium is also diffusely thickened, more than in the pre-contrast images (f, yellow circle), and has high signal related to a inverted direction of the lymphatic drainage (g-h). Coronal T1-w MIP reconstruction after 1 hour since the contrast administration, shows high signal in the thoracic duct (f,red arrow). Partial opacification of the azygos system (red arrows).

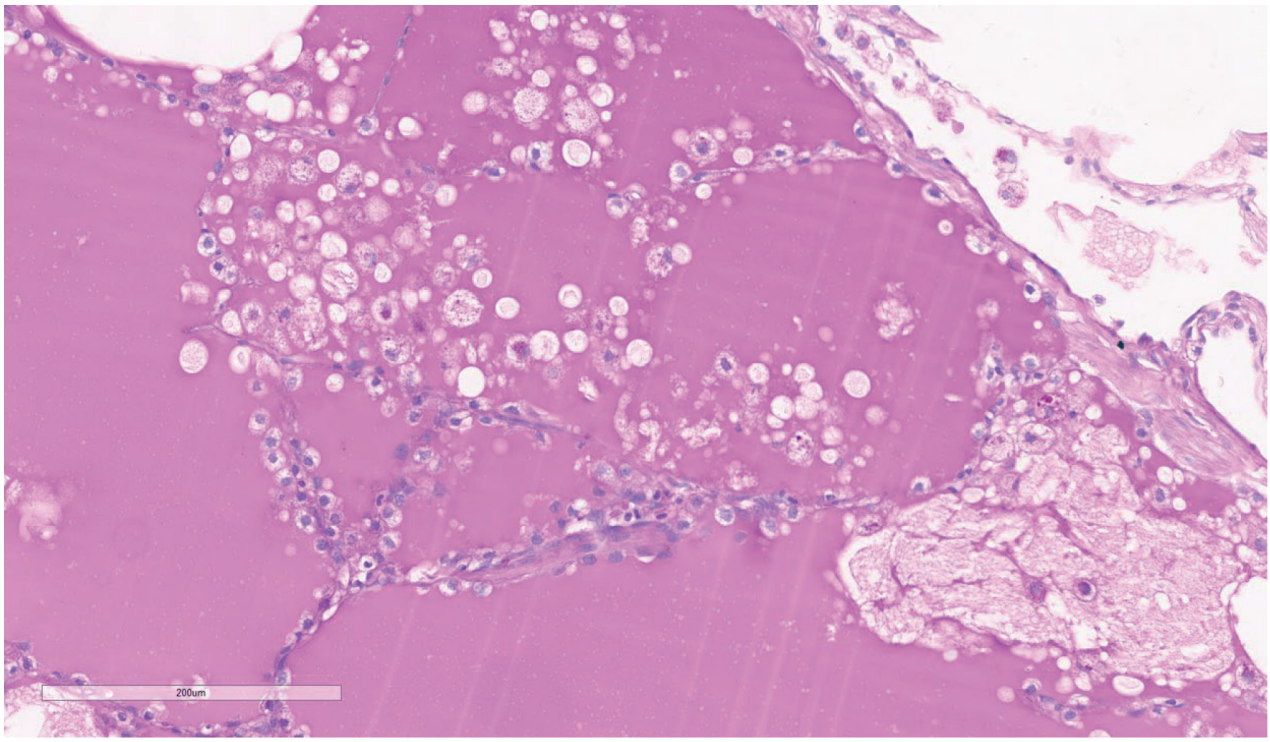

Figure 3. VATS: alveolar spaces are filled by PAS positive fluid and contain clusters of foamy macrophages (right lower corner). (PAS, x 4).

Subsequent bronchoscopy revealed whitish, tenacious plugs obstructing the left lobar bronchus, consistent with lymphatic plastic bronchitis. Given the constellation of findings, a congenital or acquired lymphatic abnormality involving the mediastinum and hilar regions was suspected. Magnetic resonance imaging (MRI) was performed following the administration of gadolinium-based contrast medium into the subcarinal (level 7), right hilar (10R), and left hilar (10L) lymph nodes under endobronchial ultrasound (EBUS) guidance.

At 30 minutes post-injection, MRI demonstrated diffuse enhancement of the mediastinal nodules, as well as marked enhancement and thickening of the peribronchovascular interstitium in both lower lobes—predominantly on the left. These abnormalities persisted in subsequent serial MRI examinations (Figure 2).

Integrating clinical, radiological, and histopathological data, a final diagnosis was established: lymphatic dysplasia of the mediastinum, characterised by the presence of multiple microlymphangiomas, lymphatic leakage into the bronchi of both lower lobes and the lower left bronchus, and associated plastic bronchitis (Figure 3).

Case 3

A 73-year-old male, former smoker with a history of occupational exposure to titanium and cobalt, presented with recent onset of dry cough, arthralgias, and an unintentional weight loss of 10 kg. ^18F-FDG PET/CT demonstrated multiple bilateral lymphadenopathies with increased metabolic activity. Chest computed tomography (CT) further revealed mild, smooth interlobular septal thickening predominantly in the mid-to-lower lung zones, associated with ground-glass opacities in the lower lobes. Laboratory investigations showed elevated transaminases and hyperbilirubinaemia. Pulmonary function testing was largely within normal limits, with the exception of a mild reduction in diffusing capacity for carbon monoxide (DLCO), measured at 63% of predicted. Given the parenchymal pattern on CT, which was not entirely characteristic of sarcoidosis, and the suspicion of coexisting lymphatic abnormalities, a cone-beam CT-guided transbronchial cryobiopsy was performed. During the same bronchoscopic session, a gadolinium-based contrast agent was administered under endobronchial ultrasound (EBUS) guidance into the 10R and 4L lymph node stations.

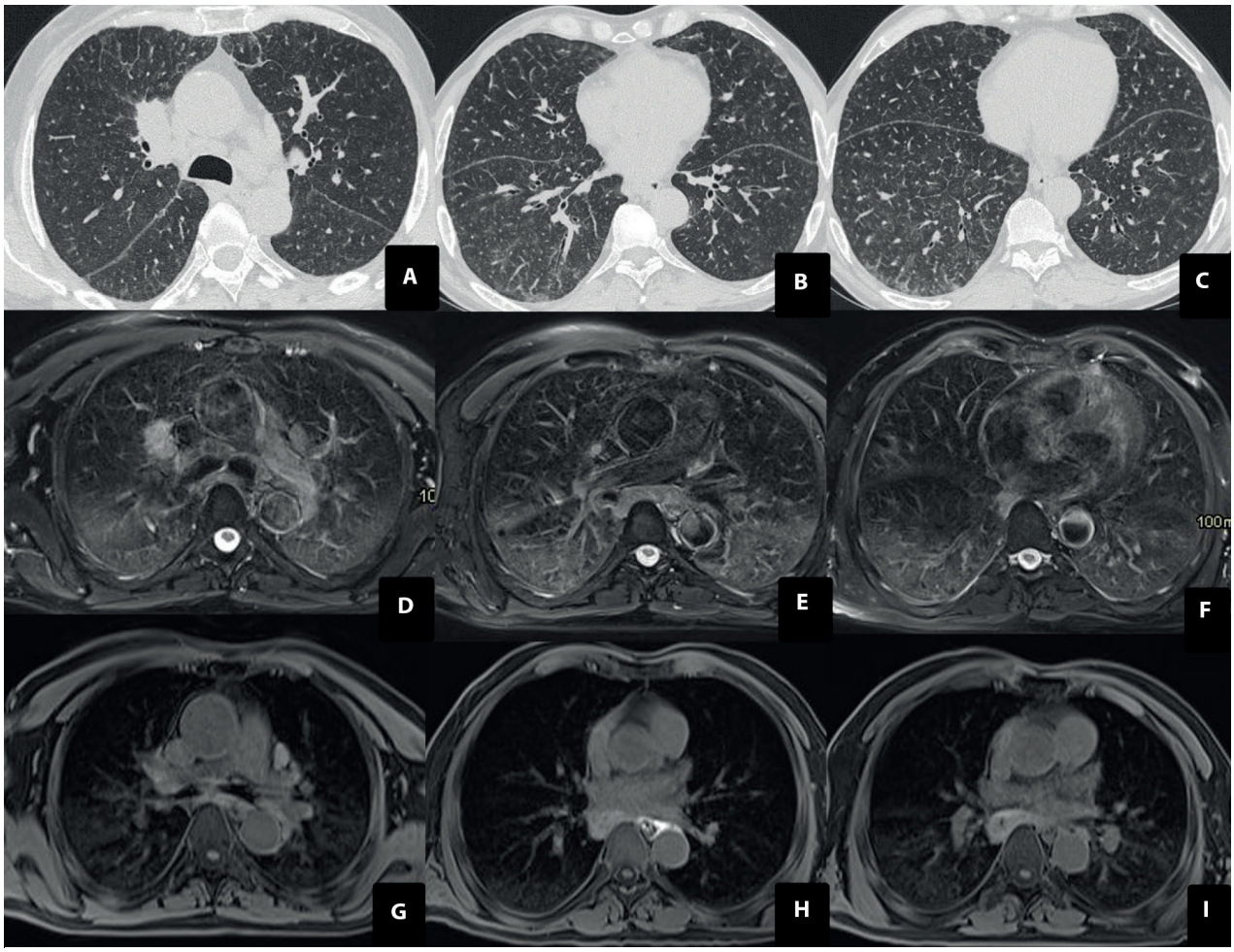

Figure 4. CT scan (a-c): nodular lesion is present in the right hilum, likely related to adenopathy. Mildly, diffusely thickened the interlobular septa, mainly in mid to lower lung zones. Mild alveolar ground glass attenuation is visibible in both lower lobes. T2w- MRI (d-f): Adenopathies in the right hilar region, and mediastinum, the biggest in subcarinal region. In both lower lobes is visible a mild increase of the signal, mainly in the left lower lobe (yellow arrow). T1w-MRI sequence with fat saturation (g-i): the first T1 image (g) was acquired before the bronchoscopy and the contrast administraion. The second T1-w image (h) was acquired twenty minutes after the end of the bronchoscopy with the contrast medium administration. It shows a minimal amount along the descending aorta. Finally, the last T1-w image was acquired one hour after the procedure, and shows findings similar to the baseline. No evidence of thickened or enhanced interstitium.

Histological evaluation of the cryobiopsy specimens revealed multiple confluent, non-necrotizing microgranulomas distributed along lymphatic pathways, consistent with a diagnosis of sarcoidosis. Subsequent magnetic resonance imaging (MRI) demonstrated normal lymphatic drainage, with no evidence of structural or functional abnormalities (Figure 4).

Discussion

The accurate visualization of mediastinal lymphatic drainage remains a significant challenge with current imaging techniques (11). The primary limitation of these methods lies in their time-consuming nature and the requirement for anatomically accessible lymph nodes. The technique we propose specifically addresses lymphatic disorders of the chest, such as thoracic duct tears (whether traumatic or due to fibrosis) or pulmonary lymphatic dysplasia.

In our first case, we successfully documented lymphatic leakage in the upper segment of the thoracic duct. In the second case, we observed an inverted flow from the central lymphatic duct to the periphery, attributable to the presence of multiple lymphangiomas (5). The third case exhibited a normal lymphatic flow.

No complications were reported, likely due to the high safety profile of gadoteric acid and the well-established safety of EBUS/EUS in the evaluation of lymphadenopathies (13). We suggest this technique should be performed in centers with a high-volume interventional pulmonology unit and advanced MR imaging capabilities.

Conclusion

In conclusion, studying lymphatic anatomy and flow mainly in the thoracic district can be particularly challenging.

The techniques involving injection of contrast agents into the inguinal lymph nodes appear to give the better results in disorders sited in the abdomen. EBUS-guided lymph node gadolinium administration might represent a promising approach in lymphatic thoracic disorders, mainly because it is easier to perform and it is faster.

Acknowledgements: The authors are very grateful to: Simona Cimini, Paolo De Rosa, Davide Lelli and Paolo Morgagni radiographers of the MR section who made feasible this study.

Conflict of Interest: The authors declare they don't have any conflict of interests.

References

1. Swartz MA. The physiology of the lymphatic system. Adv Drug Deliv Rev. 2001;50(1-2):3-20.
2. Hur S, Kim J, Ratnam L, Itkin M. Lymphatic intervention, the frontline of modern lymphatic medicine: Part I. History, anatomy, physiology, and diagnostic imaging of the lymphatic system. Korean J Radiol. 2023;2:95-108.
3. Malbrain ML, Pelosi P, De Laet I, Lattuada M, Hedenstierna G. Lymphatic drainage between thorax and abdomen: please take good care of this well-performing machinery. Acta Clin Belg. 2007; 62(Suppl 1):152-61.
4. Srinivasan A, Smith C, Krishnamurthy G, Escobar F, Biko D, Dori Y. Characterization and treatment of thoracic duct obstruction in patients with lymphatic flow disorders. Catheter Cardiovasc Interv. 2023;5:853-62.
5. Itkin MG, McCormack FX, Dori Y. Diagnosis and treatment of lymphatic plastic bronchitis in adults using advanced lymphatic imaging and percutaneous embolization. Ann Am Thorac Soc. 2016; 10:1689-96.
6. Ramirez-Suarez KI, Schoeman S, Otero HJ, Smith CL, Biko DM. State-of-the-art imaging for children with central lymphatic disorders. Semin Pediatr Surg. 2024;3:151417.
7. Chavhan GB, Lam CZ, Greer MC, Temple M, Amaral J, Grosse-Wortmann L. Magnetic resonance lymphangiography. Radiol Clin North Am. 2020;4:693-706.
8. Li XP, Zhang Y, Sun XL, et al. Lymphatic plastic bronchitis and primary chylothorax: a study based on computed tomography lymphangiography. World J Clin Cases. 2024;14:2350-8.
9. Shaikh R, Biko DM, Lee EY. MR imaging evaluation of pediatric lymphatics: overview of techniques and imaging findings. Magn Reson Imaging Clin N Am. 2019;2:373-85.
10. Gooty VD, Veeram Reddy SR, Greer JS, et al. Lymphatic pathway evaluation in congenital heart disease using 3D whole-heart balanced steady state free precession and T2-weighted cardiovascular magnetic resonance. J Cardiovasc Magn Reson. 2021;23(1):16.
11. Bordonaro V, Ciancarella P, Ciliberti P, et al. Dynamic contrast-enhanced magnetic resonance lymphangiography in pediatric patients with central lymphatic system disorders. Radiol Med. 2021;5: 737-43.
12. Brownell JN, Biko DM, Mamula P, et al. Dynamic contrast magnetic resonance lymphangiography localizes lymphatic leak to the duodenum in protein-losing enteropathy. J Pediatr Gastroenterol Nutr. 2022;74(1):38-45.
13. Poletti V, Petrarulo S, Piciucchi S, et al. EBUS-guided cryobiopsy in the diagnosis of thoracic disorders. Pulmonology. 2024;30(5):459-65.